Statistics of the longitudinal splitting of proton aurora during substorms

M. L. Gilson,[1] J. Raeder,[1] E. Donovan,[2] Y. S. Ge,[1] and S. B. Mende[3]

Received 14 March 2011; revised 5 May 2011; accepted 7 June 2011; published 27 August 2011.

[1] The lower-latitude boundary of the proton aurora, i.e., the isotropic boundary (IB), marks the transition from a full downgoing loss cone on the poleward side to an empty downgoing loss cone on the equatorward side. A number of authors have correlated this boundary with the amount of stretching in the magnetic field using GOES spacecraft. In this paper, we use 264 substorm events from the IMAGE SI-12 global proton auroral imager to show that during substorms, the proton aurora splits longitudinally 48% of the time. We hypothesize that the splitting is a result of the azimuthal growth of the substorm current wedge and show that splitting is more likely during stronger substorms (lower AL).

Citation: Gilson, M. L., J. Raeder, E. Donovan, Y. S. Ge, and S. B. Mende (2011), Statistics of the longitudinal splitting of proton aurora during substorms, *J. Geophys. Res.*, *116*, A08226, doi:10.1029/2011JA016640.

1. Introduction

[2] About thirty years ago, *Sergeev and Tsyganenko* [1982] and *Sergeev et al.* [1983] predicted that pitch angle scattering due to magnetic field line curvature could result in significant nightside proton precipitation. Specifically, regions where $R_c/\rho < \sqrt{8}$ have strong enough pitch angle scattering to fill the loss cone (R_c is the local magnetic field radius curvature and ρ is the particle gyroradius). This corresponds to the κ criterion ($\kappa = \sqrt{R_c/\rho} < 3$) used in the literature by *Büchner and Zelenyi* [1986], *Ashour-Abdalla et al.* [1990], and others. Based on this model two proton precipitation boundaries have been defined. The low-latitude proton precipitation cutoff is commonly referred to as the isotropic boundary (IB) and the maximum of the integrated precipitating energy flux is commonly referred to as the b2i. *Newell et al.* [1998] showed that the IB for 30 keV protons and the b2i are nearly identical.

[3] Generally, the IB/b2i latitude (hereafter IB_λ) measured by low altitude spacecraft is highly correlated with the degree of magnetotail stretching measured at geosynchronous orbit [*Sergeev et al.*, 1993]. The location of the IB/b2i can be inferred reasonably well from optical auroral measurements taken on the ground [*Donovan et al.*, 2003b]. *Meurant et al.* [2007] showed that IB_λ remains correlated with magnetotail stretching at geosynchronous during substorm expansion using global imaging from the SI-12 instrument [*Mende et al.*, 2000] on board the IMAGE spacecraft.

[4] Using the proton aurora and GOES data, *Meurant et al.* [2007] showed that the geosynchronous magnetic field is more stretched duskward of the substorm onset meridian. From this, they concluded that recovery probably starts in the dawn sector and propagates duskward. Apart from this, there has been very little work to investigate how the longitudinal configuration of the proton aurora can give insight to the global magnetic field topology. For example, if the proton aurora really is a good measure of the degree of stretching of the magnetotail during substorm expansion, then the IB should move poleward (or even disappear) as the substorm current wedge (SCW) [*McPherron et al.*, 1973] is formed due to the low curvature field lines inside the SCW. Demonstrating this splitting in the IB is the first purpose of this paper.

[5] The second purpose of this paper is present an index to quantify the splitting and to show how the splitting varies statistically with traditional substorm indices.

2. Data

[6] Similar to *Meurant et al.* [2007], we use the IMAGE SI-12 data for this study. The SI-12 camera used the Doppler shifted Ly-α spectral line to image the proton aurora [*Mende et al.*, 2000]. Also, in our event selection, we used the Wideband Imaging Camera (WIC) data. Generally, the WIC data represents the discrete electron precipitation since that dominates the light output during substorms although in reality, all forms of precipitation affect the WIC output [*Frey et al.*, 2003]. Both instruments took images of the aurora at approximately the same time with a cadence of about 2 min and angular resolution of 1.3×10^{-6} *sr* and 4.2×10^{-6} *sr* yielding pixel sizes of approximately 52 × 52 km and 92 × 92 km at an altitude of $7R_E$ for WIC and SI-12 respectively [*Mende et al.*, 2000].

[1]Space Science Center, University of New Hampshire, Durham, New Hampshire, USA.
[2]Department of Physics and Astronomy, University of Calgary, Calgary, Alberta, Canada.
[3]Space Science Laboratory, University of California, Berkeley, California, USA.

0148-0227/11/2011JA016640

[7] The substorms included in this study were taken from the list published by *Frey et al.* [2004]. That list contains over 2400 substorms over the northern hemisphere from May 2000 through December 2002 which were observed by the IMAGE satellite. From that list, only isolated substorms with good coverage were selected for use in the present study. To be isolated, a substorm had to be separated from any previous substorm by at least 90 min. Also, the auroral oval had to be in the camera field of view for that entire period and no more than two consecutive frames were allowed to be missing during the entire interval. Additionally, for an event to be selected, the viewing angle could not severely distort the pixel size (for substorms on the "limb" or when the pointing information was incorrect) and there had to be adequate counts to clearly distinguish the proton aurora from the background during the entire interval. The substorm also had to be clearly distinguishable in both the SI-12 and WIC images. From the original list, 356 events were selected for this study.

3. Longitudinal Splitting of Proton Aurora

[8] A large number of the events examined in this study exhibited a longitudinal splitting of the global proton aurora. For these events, the IB_λ increased locally and precipitation maxima formed duskward and dawnward of the increase. In most of these events, there was a significant decrease in the precipitation at local times corresponding to the increased IB_λ. A typical example, chosen randomly from our data set, is shown in Figure 1. Figure 1 shows six consecutive images from the SI-12 CCD during a substorm on 31 January 2001 with a onset time of about 08:26 UT. The event was a reasonably strong substorm with the provisional AL dropping to −918 nT. The raw counts are plotted in color and the position of each pixel has been mapped to solar magnetic coordinates. In the first frame (6 min after onset), the IB_λ as a function of longitude varies smoothly. In the next frame (8 min after onset), there is a slight increase of the IB_λ near the 21:00 local time meridian. In the third frame, there are two precipitation maxima with decreased precipitation in between. The fourth through sixth frames show the further development of the proton aurora including the development of the two precipitation maxima.

[9] In order to quantitatively determine which events were split, an algorithm was developed to compute a splitting index. First, meridian scans were extracted every degree in longitude on the nightside for each frame of each event. Each scan was then fit to an equation of the form

$$Counts_i = A_i e^{-\frac{(\lambda-\lambda_{\max_i})^2}{2\sigma_i^2}} + B_i \quad (1)$$

similar to *Donovan et al.* [2003b] and *Meurant et al.* [2007]. Scans where σ_i exceeded twenty degrees were removed as bad fits. Additionally, the integral of the raw counts along each scan normalized by the scan length (hereafter I_i) was computed. For each frame, the background counts was estimated as the average of all the B_i for that image. The I_i were then plotted as a function of magnetic longitude and passed through a boxcar averaging filter with a window size of ten degrees. An interactive computer program was used to find the local maximum in the filtered I_i closest to a mouse click on the satellite image for the westward and eastward precipitation maxima. The computer program then found the deepest minimum in the filtered I_i between the two fronts. The splitting index (SI) was defined as

$$\Delta I_{west,east} = I_{west,east} - I_{\min} \quad (2)$$

$$SI = \frac{\min(\Delta I_{west,east})}{counts_{background}} \quad (3)$$

where I_{east},I_{west} and $I_{\min}$ are the local extrema picked up by the computer program and $counts_{background}$ is the estimate for the background counts described above. The edges of the split region were defined to be the place where the counts had risen by half the corresponding ΔI. A simple schematic is provided in Figure 2.

[10] The integrated counts were used instead of the maximum counts because for some of the events, there was an increase in the IB_λ, but not a significant decrease in the maximum counts at the IB. In those cases, the integrated counts generally saw reduction whereas the maximum counts along a scan did not.

[11] Each event was also binned as either split or not split based on a visual inspection (red dots and green boxes in Figure 3, respectively). When the upper quartile of the not split events (green line) and the lower quartile of the split events (red line) were removed, a boundary of about 1.2 in the SI marked the transition from not split event to split event. After the removal of the quartiles and the removal of any events which existed between the upper and lower quartile SI boundaries, 264 events remained. For the events with a maximum SI greater than 1.2, we recorded the maximum width, amount of time from first splitting (SI greater than 1.2) and the amount of time until the first splitting was realized. Using AL and magnetic latitude as proxies for the substorm strength, we have investigated the correlation of these parameters with the strength of the substorm.

4. Results

[12] Of the 264 events, 128 (48%) showed clear proton auroral splitting. On average, the splitting events happened at lower AL (−614 nT versus −293 nT). A histogram of the number of events in 100 nT bins is presented in Figure 4 for events which show splitting (red) and events which do not show splitting (green). Below −600 nT (63 events), almost 94% of events exhibit splitting whereas above −200 nT (51 events), very few do (6%). In the range from −200 to −600 nT (150 events), the chance of splitting is 44%. Additionally, the moderately high correlation between maximum SI and AL (r = −0.53) also indicates that stronger events are more likely to show splitting.

[13] Generally, the onset of the split events also occurred at lower magnetic latitudes (63.2 degrees versus 65.9 degrees). Figure 5 shows the distributions of onset latitudes versus AL for events that split (red dots and trend line) versus events that did not split (green boxes and trend line). In both cases, the latitude of the onset location decreases as the AL

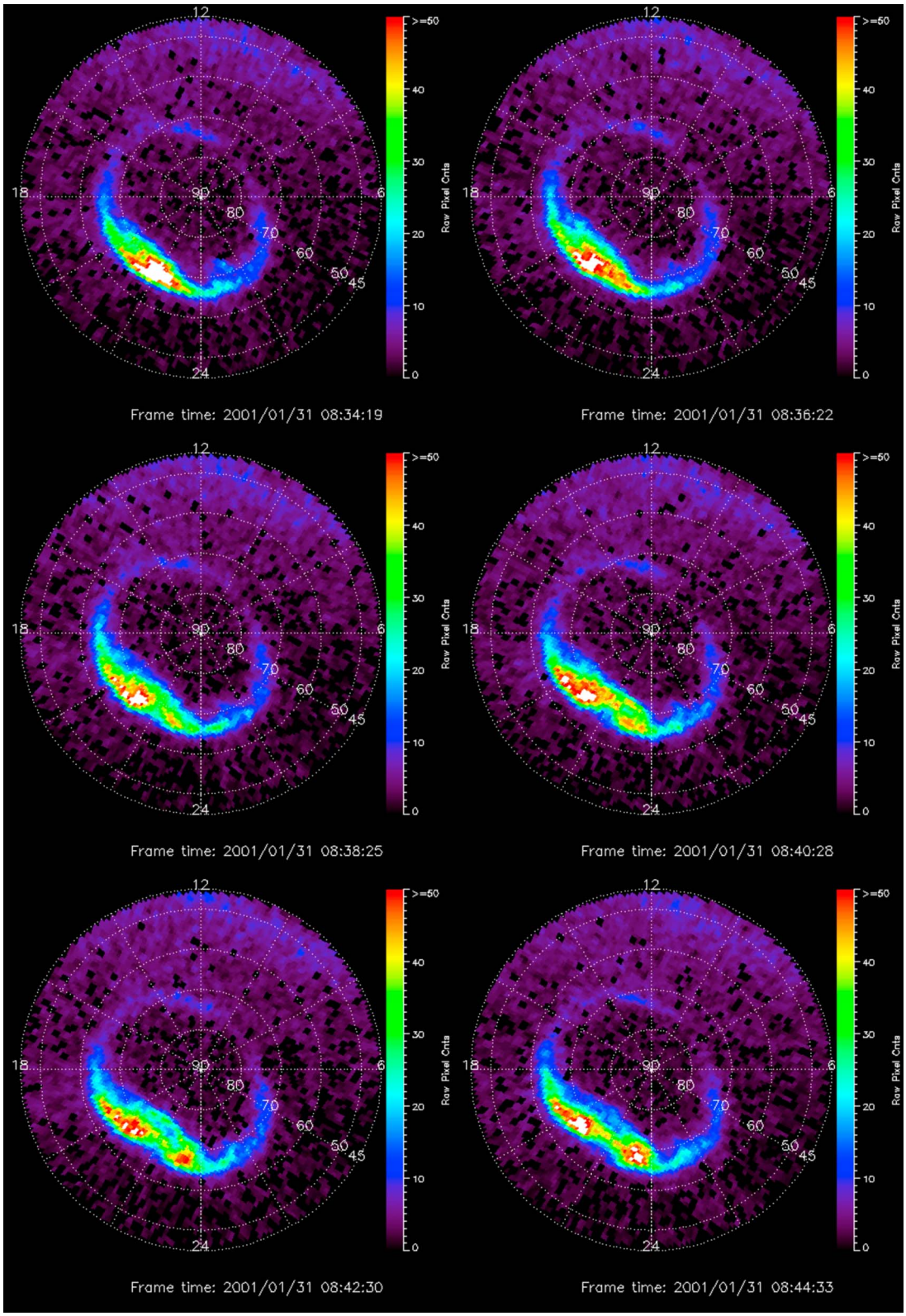

Figure 1. Splitting of the proton aurora during a substorm on 31 January 2001 as seen by the IMAGE SI-12 instrument: From left to right and top to bottom are smooth (visual) IB_λ (first panel), slight increase in the IB_λ near 21:00 (second panel), split precipitation maximum centered around 22:00 (third panel), and further development of the split region (fourth, fifth, and sixth panels). White pixels represent counts greater than 50.

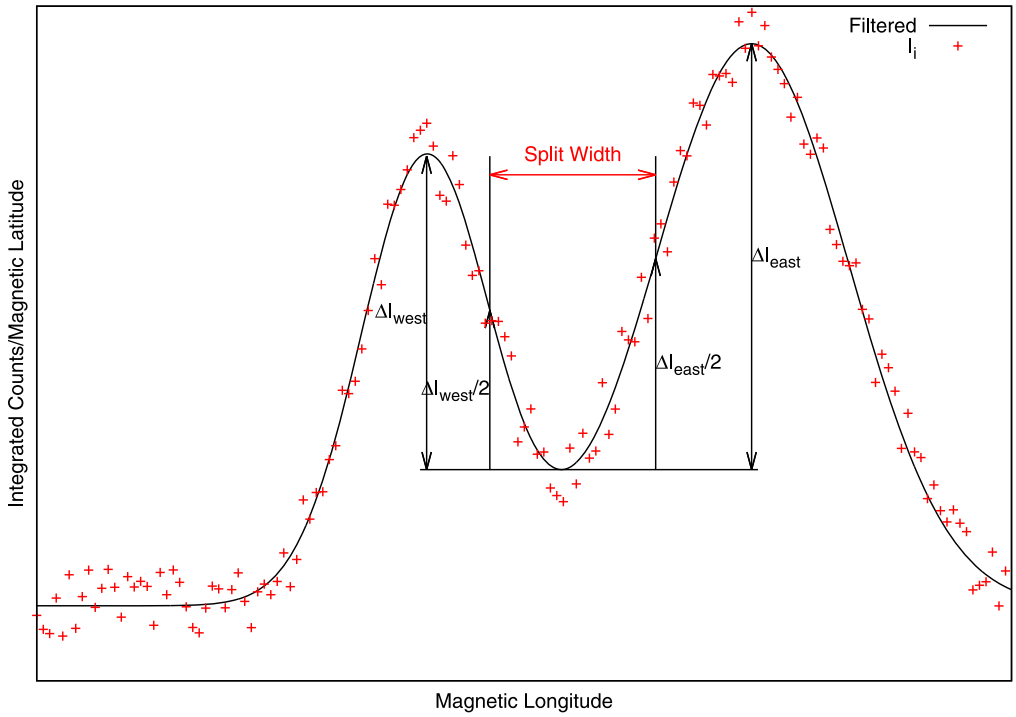

Figure 2. Schematic showing the determination of the split index and split width. For each image, meridian scans every degree in latitude were extracted. The counts along each scan were integrated and normalized by scan length. The red plus signs are representative of these integral values. The integral values are then passed through a boxcar filter (black line). The ΔI values and split width are determined as described in the text.

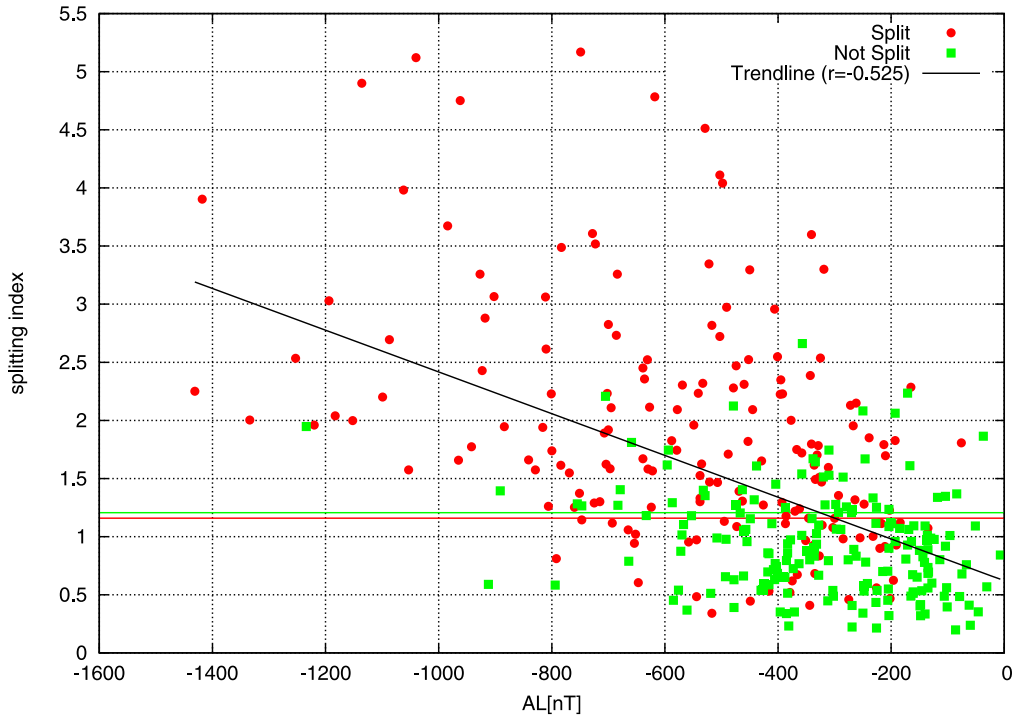

Figure 3. Maximum splitting index as a function of AL for events that were determined to be split (red dots) and not split (green boxes) by visual inspection. Red dots below the red line (split index = 1.16) represent the lower quartile of split events. Green boxes above the green line (split index = 1.2) represent the upper quartile of not split events. Both of the previously mentioned quartiles and any events between the red and green lines were removed for this study.

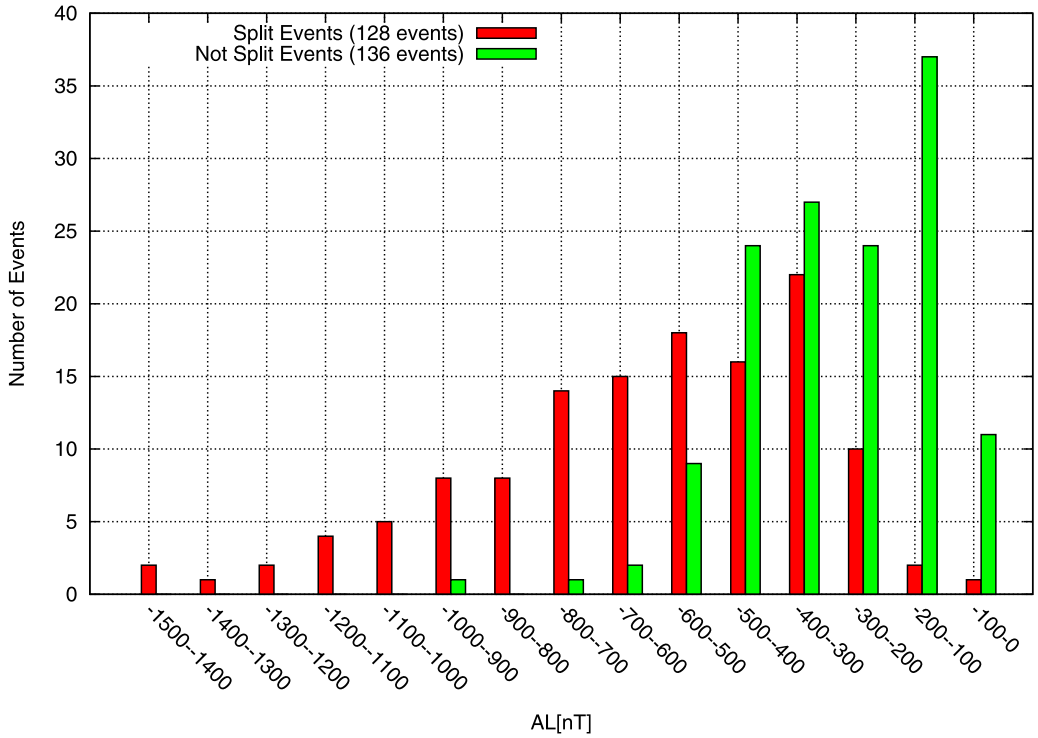

Figure 4. Histogram of the number of events that show splitting (red) and do not show splitting (green) in 100 nT bins. Generally, events which show splitting occur at lower AL than events which do not.

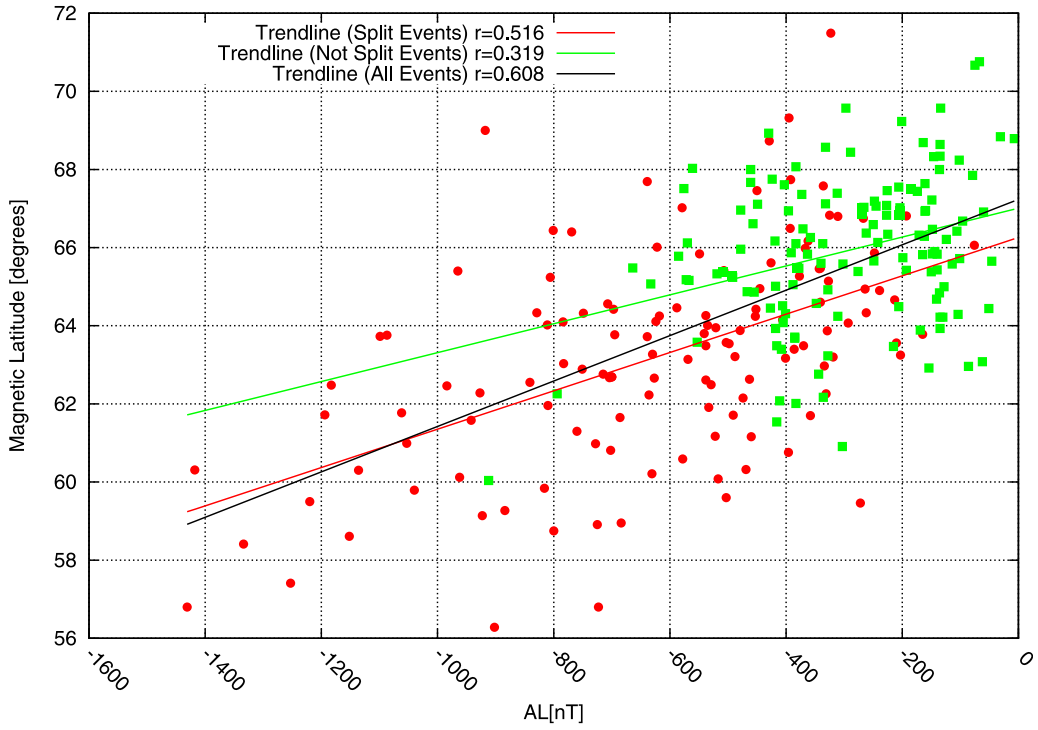

Figure 5. Onset magnetic latitude of the split events (red) and not split events (green) with trend lines. Generally, magnetic latitude decreases as AL decreases. The trend for the entire data set (black) is similar to the trend for all the events.

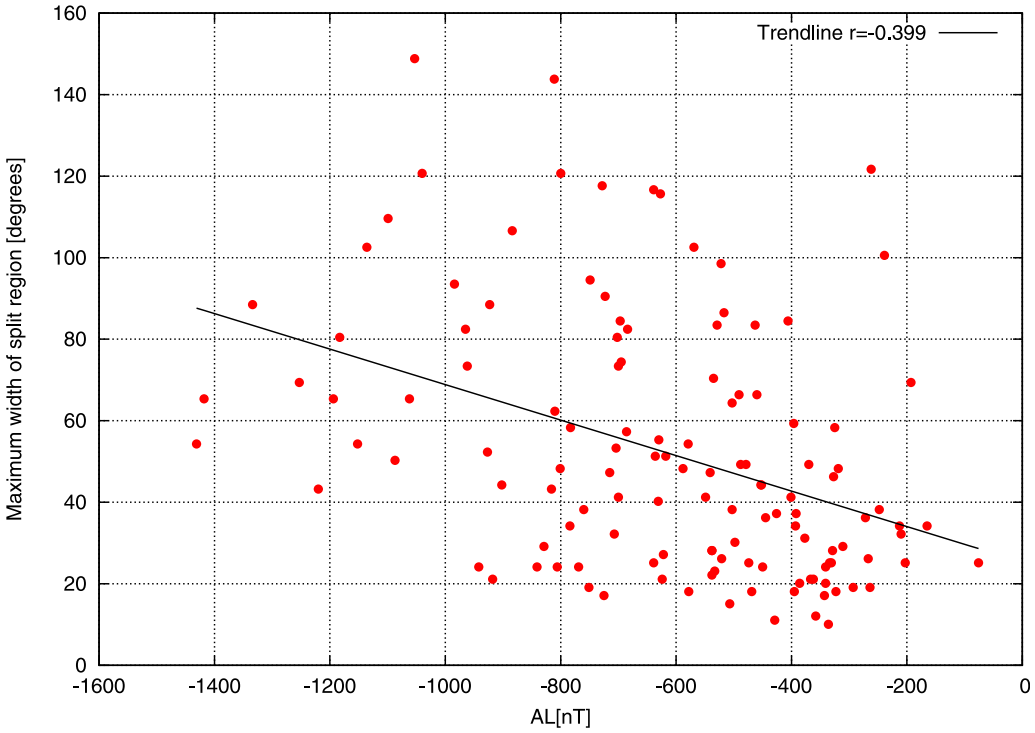

Figure 6. Maximum width of the split region as a function of AL. The moderate correlation coefficient may be the result of the repulsive force between the upward and downward field-aligned currents on the edges of the SCW.

decreases. The trend for the entire data set (both split events and not split events) has a reasonably good correlation coefficient (0.61).

[14] The maximum width of the split region was moderately anticorrelated with AL (Figure 6). On average, it took 17.5 min for the split region to reach its maximum width which was large enough to estimate the mean expansion speed. The mean expansion speed of the split region was also mostly uncorrelated (r = −0.15) with AL (Figure 7) and the average speed for all the events was 2.2 degrees longitude per minute ($27\frac{km}{s}$ in the tail at geosynchronous orbit) with only a few events having expansion speeds over 4 degrees longitude per minute ($49\frac{km}{s}$).

[15] We also investigated the timing of the splitting with respect to the onset time (Δt). Figure 8 shows the distribution of events binned by Δt along with the Δt as a function of AL. Two minute bins were chosen because that is the approximate time resolution of the data. According to the SI, only one of the events showed a clear signature of splitting prior to the onset and very few show splitting prior to 6 min after onset. However, in the visual inspection, eleven of the events appeared to be split in the same frame as the initial brightening. This indicates the SI may have difficulties when the split region is small. This discrepancy can be easily explained due to the boxcar averaging used to smooth the data in the SI determination. As such, the timing of the split determined from the SI generally is only an upper limit on the amount of time between onset and initial splitting. Events with lower AL split sooner on than events with higher AL on average, but not with a very high correlation coefficient (r = 0.18) because the events with high AL had a broad distribution of Δt.

5. Discussion

[16] The SI index described above has a number of limitations. As already mentioned, it tends to have trouble picking up small split regions. Additionally, using the integrated counts at times masked over regions where there was a clear decrease in the maximum number of counts. However, all the data results derived from the SI and split width algorithms above were also calculated based on a simple visual inspection. In general, the results showed very good agreement with the exception of the slight time shift in initial splitting.

[17] In the introduction, we hypothesized about a connection between the splitting of the proton aurora and the formation of the SCW. The statistics presented here are consistent with that view. For example, substorms with higher AL intuitively have more intense current in the SCW than their weaker counterparts because the closure of large, field aligned currents should typically result in large ionospheric currents and therefore larger ground perturbations. The larger field aligned currents are probably attributed to stronger pressure gradients [*Lui*, 1996] or enhanced magnetic shear [*Birn et al.*, 2004; *Ge et al.*, 2011] in the magnetotail due to enhanced earthward convection and/or tail flow vortices [*Keiling et al.*, 2009]. Additionally, the split generally occurs near the westward traveling surge (WTS) which is also consistent as the WTS corresponds to the most intense upward current, i.e. the westward edge of

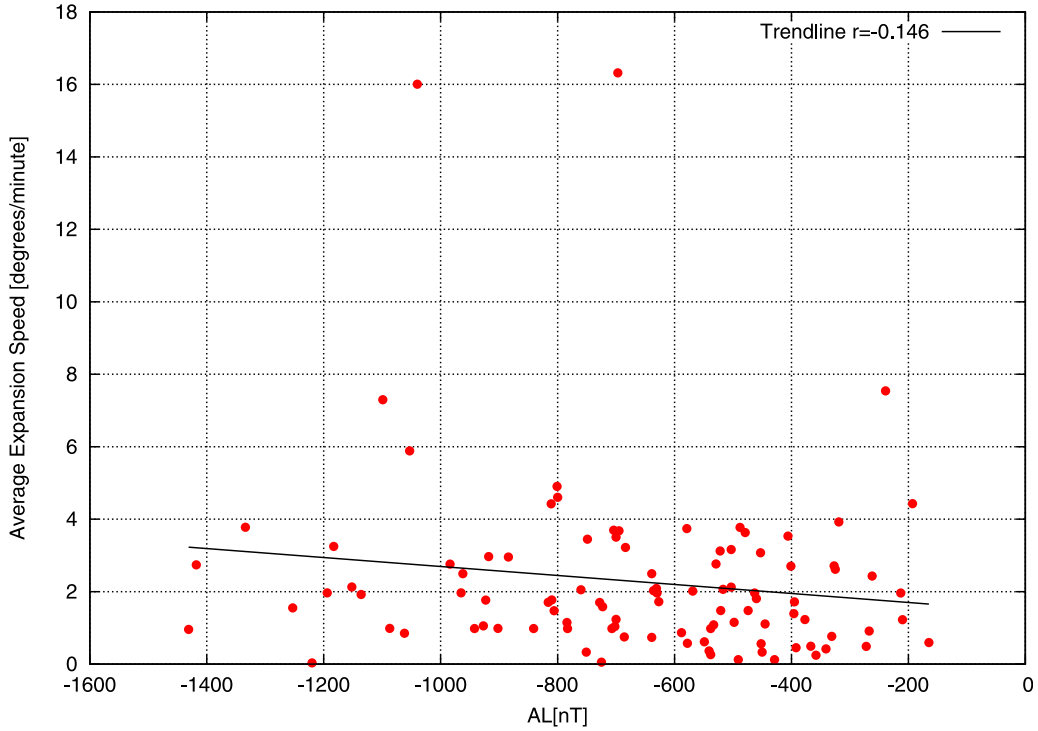

Figure 7. Average expansion speed of the split region as a function of AL. The average speed is 2.2 degrees longitude per minute, and the result is mostly uncorrelated with AL.

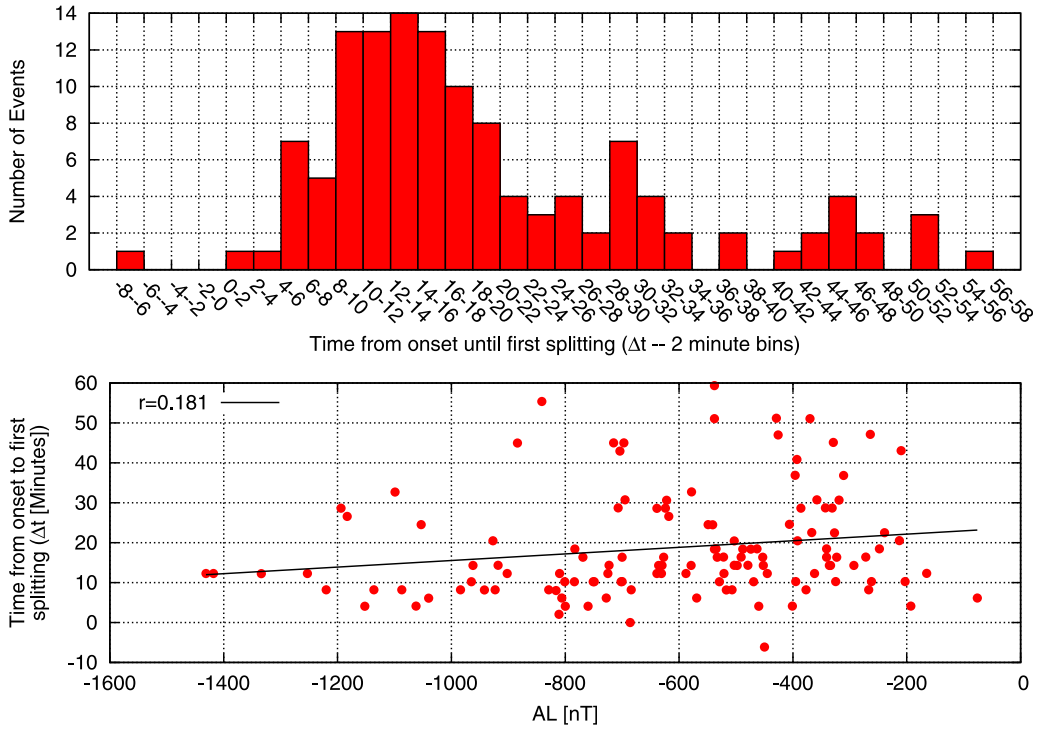

Figure 8. Time from onset until initial splitting (Δt) in two min bins. On average, events split about 17.5 min after onset. (bottom) Δt is plotted as a function of AL. Events with lower AL split sooner than events with higher AL, although with a relatively weak correlation coefficient.

the SCW [*Hoffman et al.*, 1994]. However, quantifying this relationship is difficult as there is very high variability from one substorm to the next. Some of the substorms have multiple split regions corresponding to multiple regions of bright electron precipitation, or eastward traveling electron precipitation.

[18] The moderate correlation coefficient between the maximum width of the split region and AL may also have a physical explanation if the split region corresponds to the SCW. Since the lower AL events generally occur at lower latitudes, they typically had more flux in the lobes to be reconnected. The reconnected flux would then pile up and form the SCW that is observed after the onset. It is reasonable that more reconnected flux would lead to a wider current wedge. This simple explanation neglects the very important effects of the ionospheric conductance which probably limits how good the correlation can be.

[19] It is difficult to draw conclusions about the timing of the split in the proton aurora in relation to the timing of the early formation of the substorm current wedge. This is partially due to the limitations in SI when the split region was small, but also for two additional reasons. First, proton aurora is, by nature, diffuse. As such, sharp boundaries in the precipitating energy flux do not necessarily produce sharp boundaries in the optical emissions and therefore the proton aurora will not split until a critical width of the SCW is reached. Second, the field curvature is not the only parameter affecting the precipitation. The average proton gyroradius is also important. As a result, higher energy protons should scatter off less curved field lines than lower energy protons. If the dipolarization is weak and the energization is strong, loss cone filling can still be efficient. As such, the split region in the proton aurora can only be used as a lower limit on the width of the SCW at the ionosphere. This may also explain why over half of the events did not have any clear splitting. Another possibility is that the simple cartoon picture of the SCW is not valid for all substorms.

[20] Finally, in our analysis, we have neglected all wave-particle scattering mechanisms [*Ashour-Abdalla and Thorne*, 1978]. Waves are certainly important, especially near dusk and in the afternoon sector where EMIC waves are known to cause significant proton precipitation [*Fuselier et al.*, 2004; *Yahnin and Yahnina*, 2007; *Zhang et al.*, 2008]. Closer to midnight wave-particle interactions are probably less influential; however, *Donovan et al.* [2003a] showed that the IB_λ as a function of energy is often inconsistent with the fieldline curvature mechanism assuming a simple particle distribution at the inner edge of the central plasma sheet. This result implies that either wave-particle interactions are important throughout the nightside, or that there are other processes at the inner edge of the plasma sheet that influence the distribution function there.

6. Summary and Conclusion

[21] We have shown that the longitudinal splitting of the proton aurora during substorms is a common process and we have developed an index to quantify the splitting. Our analysis demonstrates that the optical splitting is more likely to be seen in stronger substorms with lower AL (and higher magnetic latitude) and that the optical splitting is most likely to happen less than 12 min after the substorm auroral onset. These observations are consistent with a model for proton precipitation where the loss cone is filled by protons that satisfy the $\kappa = R_c/\rho < 3$ criteria. At the flanks of the SCW, there is a transition from small R_c outside to large R_c (dipolarized field) in the center. This leads to pitch angle scattering for a large range of energies outside the SCW but not inside where the field is highly dipolar resulting in a lack of proton precipitation in the center of the SCW, i.e. longitudinal splitting of the proton aurora. As the SCW grows in time, the width of the split in the proton aurora grows with it, usually at a rate of about 2.2 degrees longitude per minute regardless of AL.

[22] This study does leave some questions to be addressed in future papers. For example, why do so many of the high latitude high AL substorms avoid splitting? Perhaps the weaker substorms have current wedges further out that have less magnetic shear at the flanks. In that case, it may be possible to have curvature scattering even inside the SCW. In order to gain further understanding of how the SCW evolves outside of geosynchronous orbit, a constellation of satellites would probably be necessary. Alternatively, global modeling could be used to shed some light on the issue.

[23] Further proof for the correlation between the proton auroral splitting and the SCW could be given by looking at the ground magnetic perturbations. Specifically, there should be a correlation between the proton auroral splitting and midlatitude positive bays (MPB) [*Reddy et al.*, 1988]. This analysis could, in principle, be done by comparing existing MPB data sets and the IMAGE SI-12 data set.

[24] **Acknowledgments.** This work was supported by grant NAS5-02099 from NASA and grant ATM-0639658 from the National Science Foundation. The authors would also like to acknowledge CDAweb for providing plotting utilities and hosting IMAGE data used in this study and Larry Kepko for numerous discussions on this topic.

[25] Robert Lysak thanks Patrick Newell and another reviewer for their assistance in evaluating this paper.

References

Ashour-Abdalla, M., and R. M. Thorne (1978), Toward a unified view of diffuse auroral precipitation, *J. Geophys. Res.*, *83*, 4755–4766.

Ashour-Abdalla, M., J. Berchem, J. Buchner, and L. M. Zelenyi (1990), Chaotic scattering and acceleration of ions in Earth's magnetotail, *Geophys. Res. Lett.*, *17*, 2317–2320.

Birn, J., J. Raeder, Y. L. Wang, R. A. Wolf, and M. Hesse (2004), On the propagation of bubbles in the geomagnetic tail, *Ann. Geophys.*, *22*, 1773–1786.

Büchner, J., and L. Zelenyi (1986), Deterministic chaos in the dynamics of charged particle near a magnetic field reversal, *Phys. Lett. A.*, *118*, 395–399.

Donovan, E., B. Jackel, R. Strangeway, and D. Klumpar (2003a), Energy dependence of the latitude of the 1–25 KeV ion isotropy boundary, *Sodankylä Geophys. Obs. Publ.*, *92*, 11–14.

Donovan, E., B. Jackel, I. Voronkov, T. Sotirelis, F. Creutzberg, and N. Nicholson (2003b), Ground-based optical determination of the b2i boundary: A basis for an optical MT-index, *J. Geophys. Res.*, *108*(A3), 1115, doi:10.1029/2001JA009198.

Frey, H. U., S. B. Mende, T. J. Immel, J. C. Gerard, B. Hubert, S. Habraken, J. Spann, G. R. Gladstone, D. V. Bisikalo, and V. I. Shematovich (2003), Summary of the quantitative interpretation of image far ultraviolet auroral data, *Space Sci. Rev.*, *109*, 255–283.

Frey, H. U., S. Mende, V. Angelopoulos, and E. Donovan (2004), Substorm onset observations by IMAGE-FUV, *J. Geophys. Res.*, *109*, A10304, doi:10.1029/2004JA010607.

Fuselier, S. A., S. P. Gary, M. F. Thomsen, E. S. Clafin, B. Hubert, B. R. Sandel, and T. Immel (2004), Generation of transient dayside

subauroral proton precipitation, *J. Geophys. Res.*, *109*, A12227, doi:10.1029/2004JA010393.

Ge, Y., J. Raeder, V. Angelopoulos, M. L. Gilson, and A. Runov (2011), Interaction of dipolarization fronts within multiple bursty bulk flows in global MHD simulations of a substorm on 27 February 2009, *J. Geophys. Res.*, *116*, A00I23, doi:10.1029/2010JA015758.

Hoffman, R. A., R. Fujii, and M. Sugiura (1994), Characteristics of the field-aligned current system in the nighttime sector during auroral substorms, *J. Geophys. Res.*, *99*, 21,303–21,325.

Keiling, A., et al. (2009), Substorm current wedge driven by plasma flow vortices: THEMIS observations, *J. Geophys. Res.*, *114*, A00C22, doi:10.1029/2009JA014114. [Printed *115*(A1), 2010.]

Lui, A. T. Y. (1996), Current disruption in the Earth's magnetosphere: Observations and models, *J. Geophys. Res.*, *101*, 13,067–13,088.

McPherron, R. L., G. K. Parks, D. S. Colburn, and M. Montgomery (1973), Satellite studies of magnetospheric substorms on August 15, 1968: 2. Solar wind and outer magnetosphere, *J. Geophys. Res.*, *78*, 3054–3061.

Mende, S., H. Heetderks, H. Frey, M. Lampton, S. Geller, S. Habraken, E. Renotte, C. Jamar, P. Rochus, and J. Spann (2000), Far ultraviolet imaging from the image spacecraft. 1. System design, *Space Sci Rev.*, *91*(1), 243–270.

Meurant, M., J. Gérard, C. Blockx, E. Spanswick, E. Donovan, B. Hubert, V. Coumans, and M. Connors (2007), EL - a possible indicator to monitor the magnetic field stretching at global scale during substorm expansive phase: Statistical study, *J. Geophys. Res.*, *112*, A05222, doi:10.1029/2006JA012126.

Newell, P., V. Sergeev, G. Bikkuzina, and S. Wing (1998), Characterizing the state of the magnetosphere: Testing the ion precipitation maxima latitude (b2i) and the ion isotropy boundary, *J. Geophys. Res.*, *103*, 4739–4745.

Reddy, C. A., S. A. Kumar, and V. V. Somayajulu (1988), An observational test for the ionospheric or magnetospheric origin of night-time geomagnetic positive bays at low and mid latitudes, *Planet. Space Sci.*, *36*, 1149–1154.

Sergeev, V. A., and N. Tsyganenko (1982), Energetic particle losses and trapping boundaries as deduced from calculations with a realistic magnetic field model, *Planet. Space Sci.*, *30*, 999–1006.

Sergeev, V. A., E. Sazhina, N. Tsyganenko, J. Lundblad, and F. Soraas (1983), Pitch-angle scattering of energetic protons in the magnetotail current sheet as the dominant source of their isotropic precipitation into the nightside ionosphere, *Planet Space Sci.*, *31*, 1147–1155.

Sergeev, V. A., M. Malkov, and K. Mursula (1993), Testing the isotropic boundary algorithm method to evaluate the magnetic field configuration in the tail, *J. Geophys. Res.*, *98*, 7609–7620.

Yahnin, A. G., and T. A. Yahnina (2007), Energetic proton precipitation related to ion-cyclotron waves, *J. Atmos.Sol. Terr. Phys.*, *69*, 1690–1706.

Zhang, Y., L. J. Paxton, and Y. Zheng (2008), Interplanetary shock induced ring current auroras, *J. Geophys. Res.*, *113*, A01212, doi:10.1029/2007JA012554.

E. Donovan, Department of Physics and Astronomy, University of Calgary, 2500 University Dr., Calgary, Alberta T2N 1N4, Canada. (edonovan@ucalgary.ca)

Y. S. Ge, M. L. Gilson, and J. Raeder, Space Science Center, University of New Hampshire, 8 College Rd., Durham, NH 03824, USA. (yasong.ge@gmail.com; mgilson@artemis.sr.unh.edu; j.raeder@unh.edu)

S. B. Mende, Space Sciences Laboratory, University of California, Berkeley, CA 94720, USA. (mende@ssl.berkeley.edu)